Article

Raft Formation in Lipid Bilayers Coupled to Curvature

Sina Sadeghi,[1,*] Marcus Müller,[1] and Richard L. C. Vink[1]
[1]Institute of Theoretical Physics, Georg-August-Universität Göttingen, Göttingen, Germany

ABSTRACT   We present computer simulations of a membrane in which the local composition is coupled to the local membrane curvature. At high temperatures (i.e., above the temperature of macroscopic phase separation), finite-sized transient domains are observed, reminiscent of lipid rafts. The domain size is in the range of hundred nanometers, and set by the membrane elastic properties. These findings are in line with the notion of the membrane as a curvature-induced microemulsion. At low temperature, the membrane phase separates. The transition to the phase-separated regime is continuous and belongs to the two-dimensional Ising universality class when the coupling to curvature is weak, but becomes first-order for strong curvature-composition coupling.

INTRODUCTION

Ever since the postulation of the lipid raft hypothesis (1), understanding the lateral structure and heterogeneity of lipid bilayers has been an extremely active area of research. One line of thought is that lipid rafts (i.e., tiny domains rich in saturated lipids and cholesterol floating in an ocean of unsaturated lipids) are the result of two-phase fluid-fluid coexistence. The challenge is to explain why raft domains remain small, as opposed to growing and coalescing to minimize line tension (2,3). One hypothesis is that membranes are close to (but distinctly above, i.e., in the one-phase region of the phase diagram) the critical point of the fluid-fluid coexistence region. Hence, the correlation length is still large (i.e., significantly exceeding the size of single molecules) but macroscopic domain formation does not occur. Experiments performed on model membranes indeed reveal that such systems support critical behavior (4–6), with indications that the corresponding universality class is the expected one (7) (i.e., the one of the two-dimensional Ising model).

Although the existence of critical behavior in freestanding membranes has thus been demonstrated quite convincingly (not only in model membranes, but also in cell-derived vesicles (6,8)), the relevance of this for real cell membranes is not entirely obvious, because the latter are typically not free, but intricately connected to their environment (for instance to the cytoskeleton). Relatively recent simulations have shown that, in the presence of a cytoskeleton network, macroscopic domain formation will always be suppressed (9–12). The idea is that, assuming the cytoskeleton network to be spatially random on large scales and with a preferred affinity to one of the lipid species, a new universality class is induced, namely the one of the two-dimensional random-field Ising model. As is well known (13), the latter model does not support macroscopic domain formation at any temperature nor does it support critical behavior, and so it is not a priori obvious how the critical behavior observed in freestanding vesicles would manifest itself in the presence of a cytoskeleton network. The suppression of macroscopic lipid phase separation was recently confirmed experimentally in a model membrane coupled to an actin network (14). In yeast cells, the situation is less clear (15).

In yet another view (16,17), applicable to both free-standing and nonfree membranes, the working hypothesis is that the line tension is effectively lowered by hybrid lipids; the latter collect at the raft interface, thereby lowering the line tension in much the same way a surfactant molecule would. In the presence of hybrid lipids, the tendency of the membrane to phase-separate would thus be greatly diminished, offering an alternative explanation for the stability of lipid rafts.

Finally, the last hypothesis that we mention here is that rafts may be stabilized via a coupling between the local membrane composition and the local shape (e.g., curvature, thickness) of the membrane leaflet (18–20). For instance, it may be that regions of certain curvature sign prefer certain lipid species (the feasibility of such a coupling has been demonstrated experimentally (21,22)). This hypothesis differs from the others discussed above, because it departs from the view that the membrane is strictly flat and two-dimensional. Instead, the membrane height deviations into the third dimension now play a crucial role.

The existence of the various hypotheses (i.e., critical behavior, cytoskeleton arrested phase-separation, hybrid lipids, coupling to membrane leaflet shape) precludes a comprehensive picture of exactly what goes on in membrane raft formation. Presumably, all proposed mechanisms contribute to some extent. With this idea in mind, the purpose

Editor: Tobias Baumgart.

CrossMark

of this article is to investigate by computer simulation how membrane fluid-fluid demixing is affected by a coupling to the membrane leaflet shape. We thus focus on the combined effect of the first and last discussed hypothesis (leaving aside therefore the role of hybrid lipids and the cytoskeleton). Our foremost aim is to test the recent hypothesis of Schick in which the membrane is envisioned as a curvature-induced microemulsion (18). This hypothesis is interesting for biological applications because it accounts for transient domains of finite size (i.e., rafts) at physiological temperatures, without requiring the vicinity of a critical point. Our second aim is to consider the fate of phase-separation transitions in membranes that are coupled to curvature.

The outline of this article is as follows: We first recapitulate the essentials of Schick's hypothesis. Next, we introduce our membrane model, and describe how this model is simulated using Monte Carlo updates in Fourier space. Our results, including a careful analysis of finite-size effects, are presented, and then we give our conclusions.

THEORETICAL BACKGROUND

We consider a lipid bilayer that undergoes lateral phase separation into a liquid-ordered (lo) and liquid-disordered (ld) phase. The lo phase is characterized by a high density of saturated lipids and cholesterol, whereas the ld phase has a high density of unsaturated lipids (6,23). We assume the membrane to be planar, such that the local membrane height h, and the local composition ϕ, may be expressed as functions of the lateral coordinates x,y (Monge representation). The scalar field $\phi \equiv \phi(x,y)$ describes the local composition of, say, the upper leaflet, with the sign encoding whether the position at (x,y) is predominantly lo or ld. The free energy cost of the membrane height fluctuations is given by the Helfrich form (24), which regards the membrane as an elastic sheet with bending rigidity κ, and surface tension σ, as

$$\mathcal{H}_{\text{Helfrich}} = \int \left[\frac{\kappa}{2} (\nabla^2 h)^2 + \frac{\sigma}{2} (\nabla h)^2 \right] dxdy. \quad (1)$$

The free energy cost of the composition fluctuations is described by a fourth-order Landau expansion

$$\mathcal{H}_{\text{Composition}} = \int \left[\frac{A}{2} \phi^2 + \frac{B}{2} (\nabla \phi)^2 + C\phi^4 \right] dxdy. \quad (2)$$

The molecular asymmetry between the lo and ld phases gives rise to a curvature-composition coupling term (21,22)

$$\mathcal{H}_{\text{x}} = \gamma \int \phi \, (\nabla^2 h) dxdy, \quad (3)$$

with coupling strength γ. This coupling implies that the composition of the lower leaflet will be anticorrelated. More refined descriptions allowing for a positive correlation are presented elsewhere (19,20), but here we focus on the

most simple case. The full model is the sum of the above three Hamiltonian terms

$$\mathcal{H}^{\text{Theory}} = \mathcal{H}_{\text{Helfrich}} + \mathcal{H}_{\text{Composition}} + \mathcal{H}_{\text{x}}. \quad (4)$$

Models such as Eq. 4 have been intensely studied (25–30), and the corresponding mean-field phase diagram, depicted in Fig. 1, is well known (19,31). A two-dimensional representation is used, in which the horizontal axis denotes the strength γ of the curvature-composition coupling, and the vertical axis denotes the coefficient A of the quadratic term in the Landau expansion, Eq. 2. There are four distinct thermodynamic phases: The first one is a fluid phase, indicated by regions f_1 and f_2, which is a disordered phase characterized by exponentially decaying correlations. This phase occurs for $A > 0$ and small values of γ. The difference between regions f_1 and f_2 is that the structure factor $S(q)$ assumes its maximum at wave vector $q = 0$ in f_1, and at $q = q^*$ > 0 in f_2. We emphasize that no phase transition is associated by crossing the Lifshitz line that separates regions f_1 and f_2. Thermodynamically, the entire region, f_1 and f_2, is a single phase. For $A < 0$ and small γ, the membrane macroscopically phase separates into two coexisting phases, i.e., the lo and ld phases. A may thus be regarded as the temperature difference from the critical temperature of phase separation. At large γ, the fourth phase is observed. This is a modulated phase characterized by alternating stripes in the composition, of some characteristic wavelength.

In mean-field theory, all lines meet at the Lifshitz point (LP), located at $A = 0$ and $\gamma = \gamma_{\text{Lif}}$. In the absence of
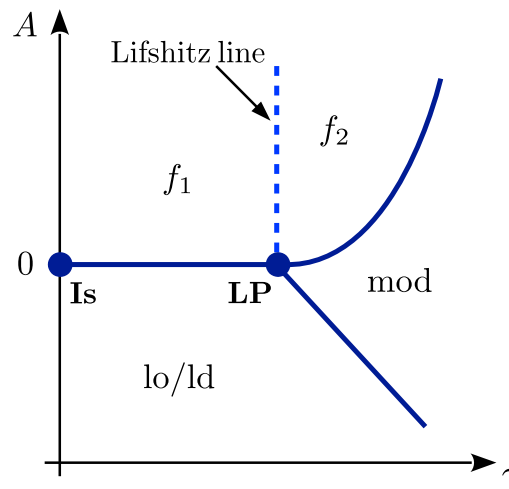

FIGURE 1 Topology of the mean-field phase diagram of Eq. 4. The horizontal axis is the strength γ of the curvature-composition coupling, the vertical axis is the prefactor A of the quadratic term in Eq. 2. There are four distinct thermodynamic phases: a disordered fluid phase spanning the regions f_1 and f_2; the lo phase and the ld phase; and a modulated phase (mod). (Solid lines) Genuine phase transitions; (dashed line) Lifshitz line. In mean-field theory, all lines meet in the Lifshitz point (LP). The point Is marks the critical point of the system without curvature-composition coupling. To see this figure in color, go online.

curvature-composition coupling, $\gamma = 0$, one recovers conventional fluid phase separation (the experimental analysis of phase separation in vesicles is typically performed this way [7]). In this case, there is a critical point (Is) below which the homogeneous fluid membrane macroscopically phase-separates into coexisting lo and ld phases. In a real membrane (accounting for fluctuations), this critical point is expected to belong to the two-dimensional Ising universality class. In the presence of curvature-composition coupling, $\gamma > 0$, the point Is marks the beginning of a line of critical points, which extends to the Lifshitz point. In mean-field theory, phase transitions between $f_1 \leftrightarrow$ lo/ld and $f_2 \leftrightarrow$ mod are continuous, whereas transitions lo/ld $\leftrightarrow$ mod are first-order.

To account for lipid rafts, i.e., composition fluctuations on a length scale that is large compared to single particles yet not macroscopic, Fig. 1 offers two possible candidates. The first is to tune the membrane close to the critical point of phase separation, i.e., just above the line "Is-LP". Provided $A > 0$, the membrane remains mixed, but with large composition fluctuations characteristic of a critical point [4,5]. The second possibility, proposed by Schick [18], is the fluid region f_2. Because the latter is above the Lifshitz line, composition fluctuations on a nontrivial scale corresponding to wave vector q^* are expected. To quantify this scale, one can ignore the quartic term in the Landau expansion ($C = 0$), because in region f_2 the coefficient $A > 0$. In terms of the Fourier components of the composition field $\tilde{\phi}(\vec{q})$, and after integrating out the height fluctuations, the free energy becomes [18]

$$\mathcal{F} = \frac{1}{2} \int \frac{|\tilde{\phi}(q)|^2}{S(q)} \, \mathrm{d}\vec{q}, \quad q = |\vec{q}|, \qquad (5)$$

with the integration over all two-dimensional wave vectors, $\vec{q}$. Here $S(q)$ denotes the static structure factor of composition fluctuations

$$\frac{1}{S(q)} = A + Bq^2 - \frac{\gamma^2}{\kappa + \sigma/q^2}. \qquad (6)$$

For $\gamma \rightarrow 0$, $S(q)$ approaches the Ornstein-Zernike form, which reaches its maximum at wave vector $q = 0$, indicating macroscopic composition fluctuations. For $\gamma > \gamma_{\mathrm{Lif}} = \sqrt{\sigma B}$, the structure factor, $S(q)$, assumes its maximum at a finite wave vector

$$q^* = \sqrt{(\sigma/\kappa)(\gamma/\gamma_{\mathrm{Lif}} - 1)}, \qquad (7)$$

and so γ_{Lif} marks the Lifshitz line (*vertical dashed line* in Fig. 1). The corresponding (inverse) value of the structure factor reads as

$$\frac{1}{S(q^*)} = A\left(1 - \frac{(\gamma - \gamma_{\mathrm{Lif}})^2}{A\kappa}\right), \qquad (8)$$

which becomes zero at $\gamma_{\mathrm{m}} = \gamma_{\mathrm{Lif}} + \sqrt{A\kappa}$ (the phase boundary $f_2 \leftrightarrow$ mod is thus parabolic).

For $\gamma_{\mathrm{Lif}} < \gamma < \gamma_m$ (region f_2), i.e., between the Lifshitz line and the modulated phase, the system resembles a microemulsion. That is, the membrane is overall disordered, but with composition fluctuations on a nontrivial length scale set by the wave vector q^*. As noted in Schick [18], this is promising in view of rafts, which are postulated to be transient domains of finite size. To obtain the actual length, one Fourier-transforms $S(q)$, which in two dimensions corresponds to a Hankel transform. The result from Schick [18] is a characteristic size of the composition fluctuations $\sim(\kappa/\sigma)^{1/2}$. For typical values of the bending rigidity and tension, this size is ~ 100 nm, which is compatible with the raft scale.

SIMULATION MODEL

Our simulation model is a discretized version of Eq. 4. It is defined on a $L \times L$ periodic square lattice, each lattice site having a spatial coordinate (i,j). To describe the membrane composition, we assign a spin variable $s_{i,j} = \pm 1$ to each cell, where the sign indicates whether the cell (i,j) is predominantly lo or ld. To incorporate the membrane height fluctuations, we also assign to each cell a real number $h_{i,j} \in \mathbb{R}$ describing the membrane height at cell (i,j) measured with respect to a flat reference plane. Without loss of generality, the reference height is placed at zero in what follows. The total free energy of our simulation model is given analogously to Eq. 4 as

$$\mathcal{H}^{\mathrm{Sim}} = \mathcal{H}_{\mathrm{Helfrich}}^{\mathrm{Sim}} + \mathcal{H}_{\mathrm{Composition}}^{\mathrm{Sim}} + \mathcal{H}_{\mathrm{x}}^{\mathrm{Sim}}. \qquad (9)$$

The first term describes the elastic energy of the membrane height fluctuations, for which we again use the Helfrich expansion [24]

$$\mathcal{H}_{\mathrm{Helfrich}}^{\mathrm{Sim}} = \sum_{(i,j)} \frac{a^2}{2} \left[\kappa \left(\nabla^2 h_{i,j}\right)^2 + \sigma \left|\nabla h_{i,j}\right|^2\right], \qquad (10)$$

where a is the lattice spacing, and with the sum over all lattice sites:

$$\sum_{(i,j)} \equiv \sum_{i=0}^{L-1} \sum_{j=0}^{L-1}.$$

The first term in Eq. 10 is the bending energy, and its strength is set by the bending modulus, κ. The latter term describes the free energy of membrane area deformations, and its scale is dictated by the membrane tension, σ. Note that Eq. 10 is given in discrete form, as is appropriate for a lattice model. To compute the gradient and Laplacian terms, we use the finite-difference expressions

$$\nabla h_{i,j} \equiv \frac{1}{2a} \begin{pmatrix} h_{i+1,j} - h_{i-1,j} \\ h_{i,j+1} - h_{i,j-1} \end{pmatrix},$$
$$\nabla^2 h_{i,j} \equiv \frac{1}{a^2} \left(h_{i+1,j} + h_{i-1,j} + h_{i,j+1} + h_{i,j-1} - 4h_{i,j}\right), \qquad (11)$$

as is commonly done in simulations (32). In the limit $a \to 0$, these finite-difference expressions exactly converge to their continuous counterparts; for finite a, however, some lattice artifacts may be present (e.g., square anisotropy). The second term models the lipid interactions, which we assume to be pairwise-additive, and are given by a simple Ising term

$$\mathcal{H}_{\text{Composition}}^{\text{Sim}} = -J \sum_{(i,j)} s_{i,j}\left(s_{i+1,j} + s_{i,j+1}\right), \qquad (12)$$

where $J > 0$ is the Ising interaction constant. This is following the approach of Veatch et al. (7), which also uses the Ising model to describe phase-separating vesicles, but without curvature coupling. The last term in the free energy describes the coupling of the local composition to the local membrane curvature, given in discrete form as

$$\mathcal{H}_{\text{x}}^{\text{Sim}} = \gamma \sum_{(i,j)} a^2 s_{i,j}\left(\nabla^2 h_{i,j}\right), \qquad (13)$$

where γ is the strength of curvature-composition coupling.

SIMULATION METHOD

Monte Carlo moves

To study the statistical mechanics of the model defined by Eq. 9, we use Monte Carlo simulation. To update the spin variables $s_{i,j}$, we employ single-spin-flip dynamics, whereby one of the lattice sites (i,j) is randomly chosen, and its spin variable inverted as $s_{i,j} \to -s_{i,j}$. The proposed flip is accepted with the Metropolis probability,

$$P_{\text{acc,flip}} = \min\left[1, e^{-\Delta\mathcal{H}/k_{\text{B}}T}\right],$$

where $\Delta\mathcal{H}$ is the free-energy difference computed according to Eq. 9, k_{B} is the Boltzmann constant, and T is the temperature. To update the height variables, $h_{i,j}$, we use a Monte Carlo move formulated in Fourier space (33,34). A change in the height variables only affects the Helfrich part and the coupling term of Eq. 9. This part of the free energy is conveniently expressed in Fourier space as

$$\mathcal{H}_{\text{Helfrich}}^{\text{Sim}} + \mathcal{H}_{\text{x}}^{\text{Sim}} = \frac{1}{L^2} \sum_{(u,v)}\left[\left(\frac{\kappa c_1^2}{2a^2} + \frac{\sigma c_2}{2}\right)\tilde{h}_{u,v}^* \tilde{h}_{u,v} - \gamma c_1 \tilde{s}_{u,v}^* \tilde{h}_{u,v}\right], \qquad (14)$$

where (*) denotes complex conjugation, and the coefficients are given by

$$c_1(u,v) \equiv 2[2 - \cos(2\pi u/L) - \cos(2\pi v/L)], \\ c_2(u,v) \equiv 1/2[2 - \cos(4\pi u/L) - \cos(4\pi v/L)]. \qquad (15)$$

We emphasize that Eq. 14 is the exact result obtained by Fourier transforming the corresponding real-space terms using the finite-difference expression of Eq. 11, i.e., the energy computed in real space is identical to that in reciprocal space. The Fourier amplitudes, $\tilde{X}$, of the spin and height variables are obtained by the two-dimensional Fourier transforms

$$\tilde{X}_{u,v} = \sum_{(i,j)} X_{i,j}\, e^{-2\pi\iota(ui+vj)/L}, \\ X_{i,j} = \frac{1}{L^2} \sum_{(u,v)} \tilde{X}_{u,v}\, e^{2\pi\iota(ui+vj)/L}, \qquad (16)$$

where $\iota = \sqrt{-1}$, and $X \in \{h,s\}$. Note that the amplitudes are not all independent, but related via complex conjugation, $\tilde{h}_{u,v}^* = \tilde{h}_{L-u,L-v}$, because Eq. 14 must be real.

In general, the mode amplitudes are complex numbers,

$$\tilde{h}_{u,v} = (hR)_{u,v} + \iota(hI)_{u,v},$$

where hR and hI denote the real and imaginary parts, respectively (to improve readability, we omit the dependence on u,v in the subsequent notation). The key point to note is that Eq. 14 is quadratic in hR and hI. Hence, in thermal equilibrium, these variables are Gaussian-distributed according to

$$P(x) \propto \exp\left[-(x - \mu_x)^2/\Gamma_x^2\right],$$

where $X \in \{hR, hI\}$. The average is given by the minimum of Eq. 14 as

$$\begin{aligned} \mu_{hR} &= \gamma c_1 \text{Re}[\tilde{s}_{u,v}]/\left(\kappa c_1^2/a^2 + \sigma c_2\right), \\ \mu_{hI} &= \gamma c_1 \text{Im}[\tilde{s}_{u,v}]/\left(\kappa c_1^2/a^2 + \sigma c_2\right), \end{aligned} \qquad (17)$$

while the variance follows from equipartition

$$\Gamma_{hR}^2 = \Gamma_{hI}^2 = \frac{1}{2}k_{\text{B}}TL^2/\left(\kappa c_1^2/a^2 + \sigma c_2\right), \qquad (18)$$

The exception is for purely real modes, for which $hI = 0$. In this case, $P(hR)$ remains Gaussian with average μ_{hR} but increased variance, $\Gamma_{hR}^2 \to 2\Gamma_{hR}^2$.

To update the height variables, a fast Fourier routine is used to compute the spin amplitudes, $\tilde{s}_{u,v}$. We then generate a new set of height amplitudes, $\tilde{h}_{u,v}$, each one drawn from its corresponding Gaussian distribution, and back-transform to obtain the real-space height variables, $h_{i,j}$. In this procedure, there is no accept/reject decision. The advantage of this MC move is that it yields a completely decorrelated set of height variables, at the expense of two (fast) Fourier transforms. In our simulations, spin flips and Fourier height moves are typically attempted in a ratio $(10L^2{:}1)$, respectively.

Order parameter distribution

In the analysis to be presented, a key role is played by the order-parameter distribution, $P(m)$, defined as the probability to observe the membrane with composition,

$$m = L^{-2} \sum_{(i,j)} s_{i,j}.$$

During the simulations, as spins are flipped, m fluctuates; $P(m)$ is the histogram of observed m values. The distribution depends on all the model parameters, including the system size L. For a system of size L, there are L^2 possible values of the composition. To accurately obtain $P(m)$, it is required that the simulation visits all of them. We used successive umbrella sampling for this purpose (35), where the range, $L^2 m = -L^2, -L^2 + 2, \ldots, L^2$, is sampled on successive steps. As the number of steps grows $\propto L^2$, this analysis is restricted to relatively small systems, $L \approx 40$. In cases where only a single snapshot is required, for instance to measure the structure factor, much larger lattices $L = 200$ can be used. To enhance efficiency, we used histogram reweighting (36) to extrapolate data obtained for given model parameters (here: J and γ) to different (nearby) values.

Model parameters and units

In what follows, we use reduced coupling constants J, κ, σ, and γ, which have a factor $1/k_{\text{B}}T$ absorbed into them. All lengths are measured in units of the lattice spacing, a. We set $\kappa = 20$ and $\sigma = 1$. With this choice, we expect $\gamma_{\text{Lif}} = \sqrt{\sigma B}$ to be of order unity. The characteristic length of the

composition fluctuations is then $l \sim (\kappa/\sigma)^{1/2} \approx 4.5$. Because this physically relevant length scale is significantly larger than our spatial discretization, $l >> a \equiv 1$, our choice mitigates lattice artifacts of the discretized curvature Hamiltonian. Yet, l is small enough such that we can investigate systems that comprise many domains, $L >> l$. If we take typical values for the membrane tension $\sigma \sim 10^{-5}$–10^{-6} N/m (18), ambient temperature $T = 300$ K, and bending rigidity $\kappa = 20 \, k_B T$, then $(\kappa/\sigma)^{1/2} \approx 90$–$300$ nm.

RESULTS

No curvature coupling: $\gamma = 0$

For $\gamma = 0$, the model defined by Eq. 9 reduces to the two-dimensional Ising model (37). In situations where the composition m can fluctuate freely, the corresponding phase behavior is as follows: For $J > J_{crit} = \ln(1 + \sqrt{2})/2 \approx 0.44$, the Ising model phase separates into two coexisting phases—one where the majority of spins are positive (composition $m > 0$), and one where they are negative (composition $m < 0$). These phases are identified as the lo phase and the ld phase. When $J < J_{crit}$, the Ising model is in the disordered fluid phase, characterized by $m = 0$. The transition, at $J = J_{crit}$, is continuous, and belongs to the two-dimensional Ising universality class. This corresponds to the point Is in Fig. 1. In cases where the composition is fixed, which is typical for experiments, the same scenario applies provided that $m = 0$. For $m \neq 0$, the transition occurs at a larger value of J and is first-order.

Fluid phase with curvature coupling

We now consider the fluid phase in the presence of curvature-composition coupling $\gamma > 0$, corresponding to regions f_1 and f_2 in Fig. 1. Because this is the one-phase region, the Ising interaction constant J is below its critical value J_{crit}. Here, we choose $J = 0.4$. In Fig. 2 a, we show the static structure factor, $S(q)$, for several γ, where

$$S(\vec{q}) = \left\langle \frac{1}{L^2} \left| \sum_{(i,j)} s_{i,j} \exp(\iota \vec{q} \cdot \vec{r}) \right|^2 \right\rangle, \qquad (19)$$

with $\vec{r} = (i,j)$, wave vectors $\vec{q} = 2\pi(u,v)/L$, and $\langle \cdot \rangle$ denoting the thermal average. Note that Fig. 2 shows the angular averaged $S(q)$, where $q = |\vec{q}|$. For $\gamma = 0$, $S(q)$ reaches its maximum at $q = 0$. When γ exceeds a threshold value γ_{Lif}, $S(q)$ reaches its maximum at a finite wave vector, $q^* = 0$. In Fig. 2 b, we compare the simulated structure factor to the mean-field prediction of Eq. 6 using $\gamma = 3$. We observe that the simulated $S(q)$ can be well fitted with the mean-field form (in fitting to Eq. 6, the ratio σ/κ was set to the value used in the simulation; A, B, and γ were the fit parameters). The threshold value of γ where q^* first becomes nonzero marks the crossing of the Lifshitz line, where the membrane goes from region $f_1 \rightarrow f_2$. The biological significance is that, once this line has been crossed, the membrane is characterized by composition fluctuations of a
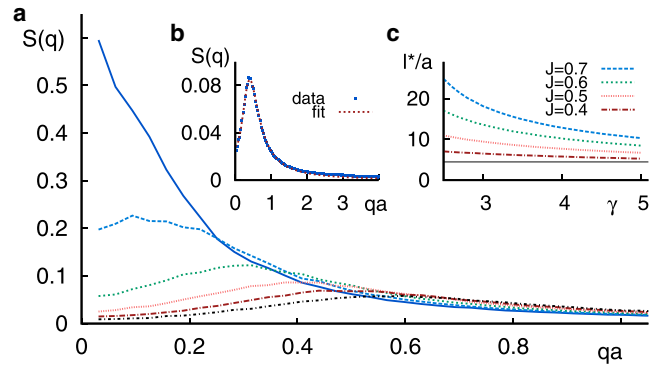

FIGURE 2 Membrane structure in the disordered fluid phase, i.e., regions f_1 and f_2 of the phase diagram (data for $J = 0.4$, $L = 200$, with the lattice constant a as the unit of length). (a) Static structure factor, $S(q)$, for curvature-composition coupling, $\gamma = 0, 1, 2, 3, 4, 5$ (from top to $bottom$). When $\gamma = 0$, $S(q)$ assumes its maximum at $q = 0$, characteristic of region f_1. When $\gamma > \gamma_{Lif}$, the maximum occurs at a finite value, $q^* > 0$ (region f_2), and shifts to larger q as γ increases. In region f_2, the membrane resembles a raft phase, with composition fluctuations of typical size l^*. (b) Comparison between the simulated $S(q)$ (data) and the mean-field form Eq. 6 for $\gamma = 3$ (fit). (c) l^*, as computed via Eq. 20, as a function of γ, for several values of J. As γ increases, the curves approach the theoretical estimate $\sim(\kappa/\sigma)^{1/2}$ (18) (indicated by the $horizontal$ $line$). To see this figure in color, go online.

characteristic size $l^* = 2\pi/q^*$. In simulations, it is convenient to measure l^* numerically using the formula (38)

$$l^* = 2\pi \frac{\int S(q) dq}{\int q S(q) dq}. \qquad (20)$$

Fig. 2 c shows l^* versus γ for various values of J. As γ increases, the curves approach to a common value. Schick (18) predicts this length to be of $\sim(\kappa/\sigma)^{1/2}$, marked with the horizontal line. The presence of a characteristic length scale l^* may also be inferred from simulation snapshots that are presented in Fig. 3. Shown are typical membrane configurations, for two values of γ, and several values of J.

Next, we ask whether the raft domains are functional, i.e., be able to serve as platforms for biologically relevant tasks. To this end, there should be a composition contrast between the raft domains, and the surrounding host phase. To show the contrast, we performed a grid analysis at $J = 0.43$ and $\gamma = 1$. For $\gamma = 1$, macroscopic lo/ld phase separation occurs when $J \gtrsim 0.51$ (evidence is presented in the next section). Hence, $J = 0.43$ is deep inside the fluid region f_2 of the phase diagram, well away from the lo/ld coexistence region ($J = 0.43$ is even below J_{crit} of the two-dimensional Ising model). In the grid analysis, a $w \times w$ cell is selected randomly from the snapshot, and the (normalized) composition

$$\overline{m} = (1/w^2) \sum_{i \in cell} s_i$$

in that cell is recorded. One then repeats this procedure for different random locations in a snapshot and different snapshots along the simulation trajectory, and constructs a
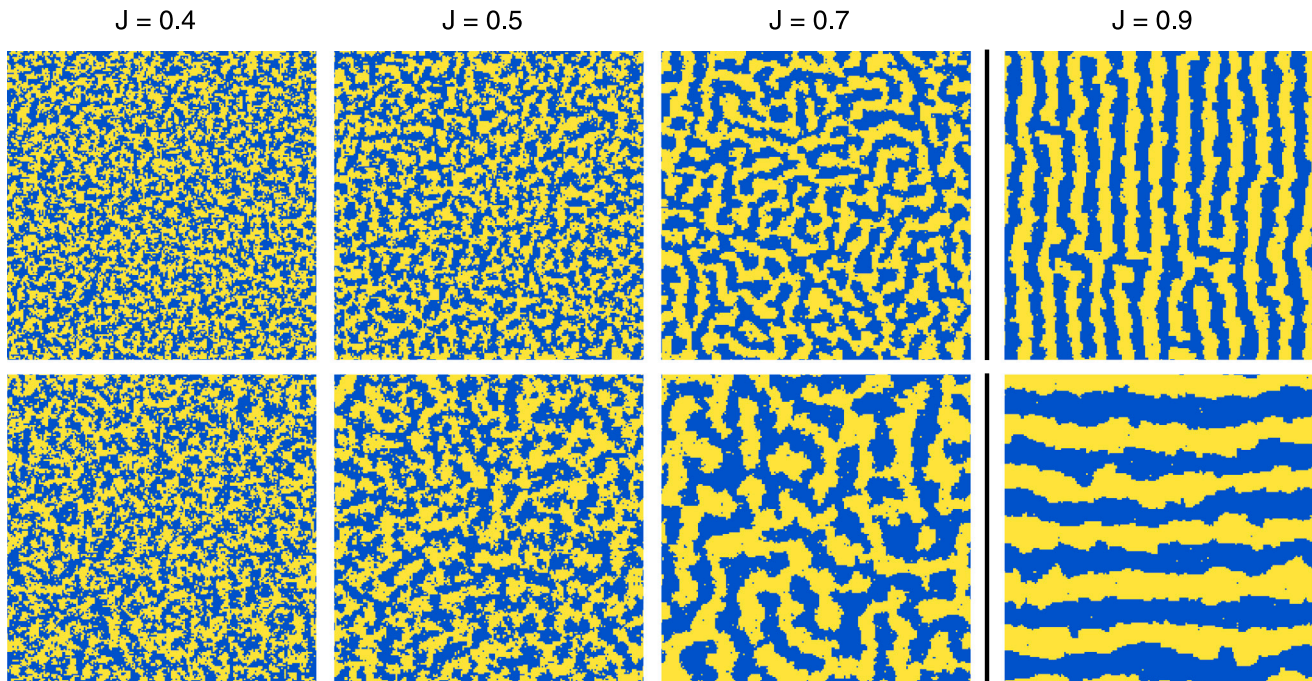
FIGURE 3 Typical membrane configurations, for several values of J, and for two values of the curvature-composition coupling, namely $\gamma = 5$ (*top row*) and $\gamma = 3$ (*lower row*). The lattice size is $L = 200$. (*Blue*) Lo domains; (*yellow*) ld domains. The snapshots left of the vertical line ($J \leq 0.7$) correspond to the raft region f_2 of the phase diagram of Fig. 1. In this case, the membrane is characterized by composition fluctuations of typical size $\sim(\kappa/\sigma)^{1/2}$ (18), but there is no long-range order. The snapshots at $J = 0.9$ show modulated phases (region *mod* of Fig. 1), where the domains have crystallized into lamellae (in two dimensions, we do not expect the orientational order to be long-ranged, but rather to decay algebraically with system size (37)). To see this figure in color, go online.

histogram $H(\overline{m})$ of the observed composition values on the length scale, w. In Fig. 4, we show how $H(\overline{m})$ depends on the grid size, w. For small w, the histograms are distinctly bimodal, whereas for large w a single peak is observed. For w corresponding to the raft size, which for our parameters is ~4.5, $H(\overline{m})$ is still bimodal, showing that raft domains ($\overline{m} \sim +1$) are clearly resolved from the surrounding phase ($\overline{m} \sim -1$). The results of Figs. 2 and 4 provide a numerical confirmation of Schick's hypothesis (18). If composition is coupled to curvature, there indeed exists a fluid phase, f_2,

with composition fluctuations compatible with the raft scale. This fluid phase persists well away from the lo/ld coexistence region, i.e., it does not require the membrane to be tuned close to a critical point.

Phase transitions

As stated above, for $\gamma = 1$ and $J \gtrsim 0.51$, the membrane is in the lo/ld coexistence region. This conclusion is based on the order-parameter distribution, $P(m)$, introduced in Order
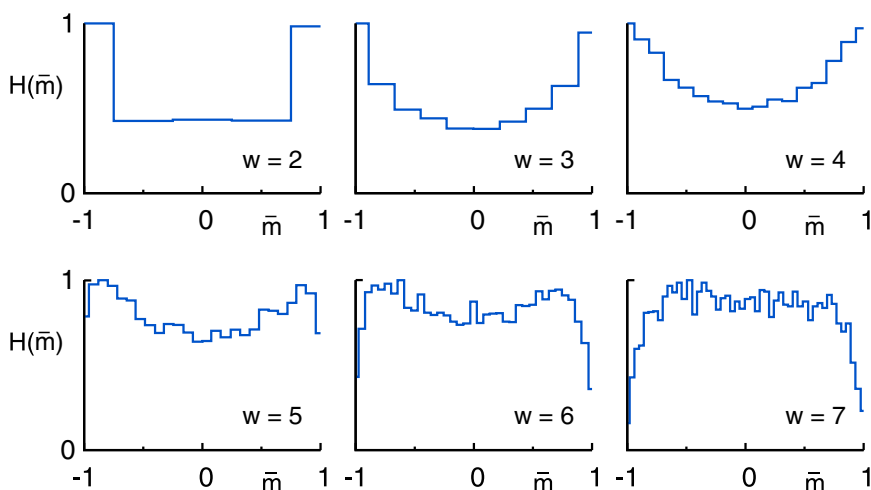

FIGURE 4 Results of a grid analysis at $J = 0.43$ and $\gamma = 1$ showing the histogram $H(\overline{m})$ of the normalized composition $\overline{m}$ measured in $w \times w$ cells. For w in the range of the raft size $\sim(\kappa/\sigma)^{1/2} = 4.5$, the histograms remain distinctly bimodal, implying a clear contrast between raft domains ($\overline{m} \sim +1$) and the surrounding host phase ($\overline{m} \sim -1$). To see this figure in color, go online.

Parameter Distribution. In Fig. 5 (*main panel*), we show ln$P(m)$ for $\gamma = 1$ and $J = 0.53$. We observe a pronounced bimodal distribution, featuring two sharp peaks symmetrically distributed around $\sim m = 0$. This bimodal shape is the hallmark of two-phase coexistence (39), each peak representing one phase—in this case, the lo and ld phases. To ensure that the observed bimodal shape is not a finite-size artifact, Fig. 5 (*inset*) shows how the free-energy barrier ΔF (*double arrow*) scales with the lattice size. As L increases, ΔF linearly increases, providing further confirmation of genuine lo/ld coexistence (40). The slope, $\Delta F/2L > 0$, quantifies the line tension between the two laterally coexisting phases (41).

In mean-field theory, the transition between the fluid and the lo/ld coexistence region is continuous. Our simulations, in contrast, reveal that the latter transition becomes first-order, provided γ is large enough. To quantify this, we study the composition fluctuation

$$\chi = L^2 \left(\langle m^2 \rangle - \langle |m| \rangle^2 \right)$$

(42), with averages defined as

$$\langle f(m) \rangle = \int f(m) P(m) \, dm.$$

In Fig. 6 *a*, we plot χ versus J for various lattice sizes L at $\gamma = 1$. For each curve, there is a value $J = J_L$, where χ reaches its maximum χ_L. The observation of a maximum in the composition fluctuation is the hallmark of a phase transition. However, phase transitions are defined only in the thermodynamic limit $L \to \infty$, and so we must carefully check how our data scale with L. Finite-size scaling theory (38,39,43,44) predicts that $\chi_L \propto L^r$, with $r = 7/4$ if the transition is critical and of the two-dimensional Ising universality class, and $r = D = 2$ if the transition is first-order with D being the spatial dimension. In Fig. 6 *b*, we plot χ_L versus L on double logarithmic scales. The expected power-law scaling is strikingly confirmed, with an exponent, $r \approx 2.0$,
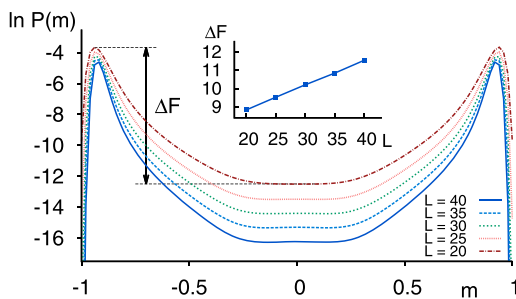
FIGURE 5 Simulation evidence showing that, for $J = 0.53$ and $\gamma = 1$, the membrane is in the two-phase lo/ld coexistence region. (*Main panel*) Probability distribution, ln$P(m)$, for several system sizes, L. The distributions are distinctly bimodal. (*Vertical double-arrow*) For $L = 20$, defining the barrier ΔF. (*Inset*) ΔF versus L; a linear increase is observed, consistent with the expected scaling for coexistence in $D = 2$ dimensions (40). To see this figure in color, go online.
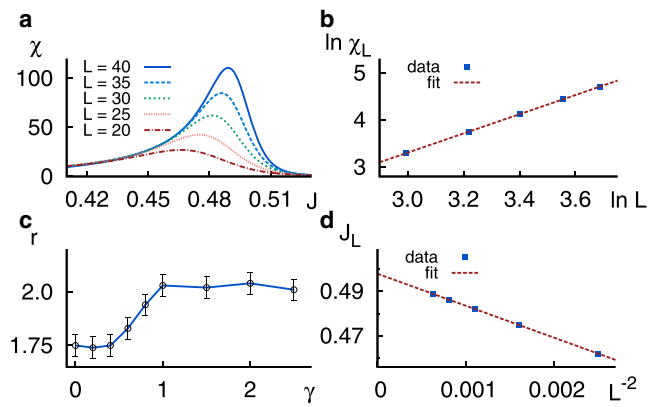
FIGURE 6 Finite-size scaling analysis of the phase transition between the lo/ld coexistence region and the fluid phase. (*a*) The composition fluctuation χ versus J for various system sizes L and $\gamma = 1$. The pronounced peak, at $J = J_L$, and the increase of the peak height χ_L with L, indicates that a phase transition occurs. (*b*) The scaling of the maximum composition fluctuation lnχ_L with ln$L$ for $\gamma = 1$. The linear increase indicates a power-law $\chi_L \propto L^r$, with $r \sim 2.0$ obtained by fitting. This shows that the transition for $\gamma = 1$ is first-order. (*c*) The exponent r versus γ. For large γ, the transition is first-order ($r = 2$), whereas lower values of γ reveal a continuous transition approaching $r = 7/4$ of the two-dimensional Ising model. (*d*) J_L versus L^{-2} for $\gamma = 1$. (*Dashed line*) Linear fit, whose intercept yields J_∞ of the thermodynamic limit. To see this figure in color, go online.

obtained by fitting. Hence, our scaling analysis indicates that for $\gamma = 1$ the transition is first-order. In Fig. 6 *c*, we plot r versus γ. For small γ, the exponent, r, approaches the two-dimensional Ising value. This is to be expected because, for $\gamma = 0$, Eq. 9 is the Ising model.

From this simulation evidence, we propose the following scenario for the transition between the fluid phase and the lo/ld coexistence region: In the absence of curvature-composition coupling, $\gamma = 0$, the transition is continuous and of the two-dimensional Ising class. For large γ, the transition is first-order. Hence, there is a special intermediate value, $\gamma = \gamma_{tri}$, where the type of the transition changes from continuous to first-order—in the language of phase transitions, this is called a tricritical point (45). In the thermodynamic limit, we thus expect that $r = 7/4$ for $\gamma < \gamma_{tri}$, and $r = 2$ for $\gamma > \gamma_{tri}$. The smooth variation of r depicted in Fig. 6 *c* indicates that the systems considered by us are too small to see the asymptotic scaling behavior. In these situations, one observes crossover scaling (46), which is characterized by effective exponents in-between the Ising and first-order values. Hence, a precise determination of γ_{tri} is not possible, but we estimate $\gamma_{tri} \approx 0.6$–1.0 because the slope of r versus γ changes most rapidly in this interval. The reason that prevents us from locating the tricritical point more precisely is the requirement that L must be large compared to the physical length scale $(\kappa/\sigma)^{1/2} \sim 4.5$ of the noncritical composition fluctuations. In terms of the latter length, our simulated systems are clearly very small, and so we cannot reach the accuracy that is typical for studies of tricritical behavior using simpler models (47).

Finally, we present the simulated phase diagram, in the regime of small γ. For each γ, the inverse transition temperature, J_∞, in the thermodynamic limit was obtained using the finite-size scaling formula $J_\infty - J_L \propto 1/L^s$. For the two-dimensional Ising model, $s = 1$, whereas for a first-order transition, $s = D = 2$. In Fig. 6 d, we show the result of the corresponding linear fit for $\gamma = 1$ using $s = 2$; the intercept yields J_∞. Because γ_{tri} is not precisely known, it is not clear which value of s to use in the extrapolation. However, the resulting estimates do not sensitively depend on s. We therefore performed the fit for both values, and report for J_∞ the average value. The resulting phase diagram is presented in Fig. 7, which shows $1/J_\infty$ versus γ. This curve separates the fluid phase from the lo/ld coexistence region, and it is the simulation analog of the mean-field phase diagram of Fig. 1 for small values of γ. Note that Fig. 7 does not show the transitions toward the modulated phase, which one expects for large J and large γ (see the snapshots for $J = 0.9$ in Fig. 3 or, alternatively, the experiments in Toulmay and Prinz (48)). The analysis of the $f_2 \leftrightarrow$ mod transition is very demanding numerically and not attempted here (due to the large value of J, the accept rate of the spin-flips will be low). We merely remark that, if fluctuations are taken into account, the transition $f_2 \leftrightarrow$ mod will shift to larger values of J and γ, i.e., the region f_2 is expected to be larger than the mean-field estimate of Fig. 1 because thermal fluctuations extend the stability of the disordered phase at the expense of the spatially modulated phase.

CONCLUSIONS

In this article, we have presented computer simulations of a phase-separating membrane, in which the local composition was coupled to the local membrane curvature. There are two central conclusions to be drawn from this work, as follows.

The first conclusion is the numerical confirmation of the theoretical hypothesis (18) that curvature-composition coupling can induce a disordered fluid phase with a structure
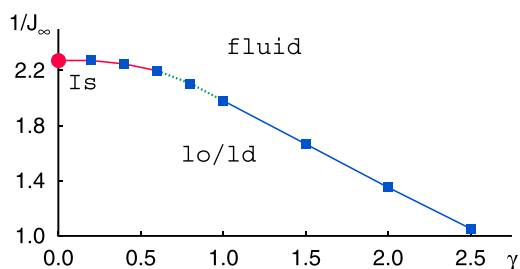

FIGURE 7 The simulated phase diagram of Eq. 9 in the regime of small γ. Plotted is $1/J_\infty$ versus γ, which separates the fluid phase from the lo/ld coexistence region (*squares* indicate the results of our finite-size scaling analysis, the *dot* marks the exact location of the two-dimensional Ising critical point). For $\gamma < \gamma_{tri}$ ($\gamma > \gamma_{tri}$), the transition between the fluid and the lo/ld region is two-dimensional Ising-critical (first-order). Based on the scaling analysis of Fig. 6 c, we estimate the tricritical point to be ~ γ_{tri} ~ 0.6–1.0. To see this figure in color, go online.

factor, whose maximum occurs at a finite wave vector $q^* > 0$. The associated length scale is set by the elastic properties of the membrane, in this case, the bending rigidity κ and the surface tension σ. For typical values of κ and σ, the characteristic scale $(\kappa/\sigma)^{1/2} \approx 100$ nm, which is compatible with the size of lipid rafts. For biological applications, it is interesting that these curvature-stabilized rafts survive at high temperature, i.e., well above the temperature of lo/ld phase separation. Hence, it is not necessary for the membrane to be tuned close to any phase transition. Admittedly, the 100-nm raft scale of this model is on the high end (49). However, alternative models are easily formulated, for instance by coupling the composition to the bilayer thickness (20). This leads to a mathematically similar model, sharing the same generic phase diagram (31), but with a numerically smaller raft size. The purpose of this article, however, was not to precisely reproduce the raft size, but rather to demonstrate how the generics of membrane phase separation are affected by a coupling to membrane shape.

Our second main result concerns the nature of the transition from the fluid phase to the lo/ld coexistence region. Provided the curvature-composition coupling, γ, is large enough, this transition becomes first-order, whereas for small γ, the transition is two-dimensional Ising-critical. The observation of a first-order transition at large γ is consistent with results obtained for microemulsions (50), as well as recent simulations of a Landau-type model (51). This result is important because membrane phase separation is typically assumed to be a continuous transition belonging to the universality class of the two-dimensional Ising model. As our data show, this assumption may not be justified in situations where membrane composition and curvature are coupled.

Finally, we wish to emphasize the importance of finite-size scaling in the analysis of phase transitions. The systematic investigation of how results depend on system size is not yet standard in biophysics. This can have several consequences, an extreme example being the false identification of phase transitions, as has occurred for the Pink membrane model (52,53). Furthermore, in biophysical applications, it could even be that experiments are affected by finite sizes. For instance, a typical fluorescence image spans ~1 μm, which is not that much larger than the 100-nm raft scale of this model.

REFERENCES

1. Simons, K., and E. Ikonen. 1997. Functional rafts in cell membranes. *Nature.* 387:569–572.

2. Lenne, P.-F., and A. Nicolas. 2009. Physics puzzles on membrane domains posed by cell biology. *Soft Matter.* 5:2841–2848.

3. Komura, S., and D. Andelman. 2014. Physical aspects of heterogene-ities in multi-component lipid membranes. *Adv. Colloid Interface Sci.* 208:34–46.

4. Veatch, S. L., O. Soubias, …, K. Gawrisch. 2007. Critical fluctuations in domain-forming lipid mixtures. *Proc. Natl. Acad. Sci. USA.* 104:17650–17655.

5. Connell, S. D., G. Heath, …, A. Kisil. 2013. Critical point fluctuations in supported lipid membranes. *Faraday Discuss.* 161:91–150.

6. Veatch, S. L., P. Cicuta, …, B. Baird. 2008. Critical fluctuations in plasma membrane vesicles. *ACS Chem. Biol.* 3:287–293.

7. Honerkamp-Smith, A. R., P. Cicuta, …, S. L. Keller. 2008. Line ten-sions, correlation lengths, and critical exponents in lipid membranes near critical points. *Biophys. J.* 95:236–246.

8. Levental, I., F. J. Byfield, …, P. A. Janmey. 2009. Cholesterol-depen-dent phase separation in cell-derived giant plasma-membrane vesicles. *Biochem. J.* 424:163–167.

9. Fischer, T., and R. L. C. Vink. 2011. Domain formation in membranes with quenched protein obstacles: lateral heterogeneity and the connec-tion to universality classes. *J. Chem. Phys.* 134:055106.

10. Fischer, T., H. J. Risselada, and R. L. C. Vink. 2012. Membrane lateral structure: the influence of immobilized particles on domain size. *Phys. Chem. Chem. Phys.* 14:14500–14508.

11. Machta, B. B., S. Papanikolaou, …, S. L. Veatch. 2011. Minimal model of plasma membrane heterogeneity requires coupling cortical actin to criticality. *Biophys. J.* 100:1668–1677.

12. Ehrig, J., E. P. Petrov, and P. Schwille. 2011. Near-critical fluctuations and cytoskeleton-assisted phase separation lead to subdiffusion in cell membranes. *Biophys. J.* 100:80–89.

13. Imry, Y., and S. K. Ma. 1975. Random-field instability of the ordered state of continuous symmetry. *Phys. Rev. Lett.* 35:1399–1401.

14. Honigmann, A., S. Sadeghi, …, R. Vink. 2014. A lipid bound actin meshwork organizes liquid phase separation in model membranes. *eL-ife.* 3:e01671.

15. Spira, F., N. S. Mueller, …, R. Wedlich-Söldner. 2012. Patchwork organization of the yeast plasma membrane into numerous coexisting domains. *Nat. Cell Biol.* 14:640–648.

16. Yamamoto, T., and S. A. Safran. 2011. Line tension between domains in multicomponent membranes is sensitive to degree of unsaturation of hybrid lipids. *Soft Matter.* 7:7021–7033.

17. Palmieri, B., and S. A. Safran. 2013. Hybrid lipids increase the proba-bility of fluctuating nanodomains in mixed membranes. *Langmuir.* 29:5246–5261.

18. Schick, M. 2012. Membrane heterogeneity: manifestation of a curva-ture-induced microemulsion. *Phys. Rev. E Stat. Nonlin. Soft Matter Phys.* 85:031902.

19. Shlomovitz, R., and M. Schick. 2013. Model of a raft in both leaves of an asymmetric lipid bilayer. *Biophys. J.* 105:1406–1413.

20. Meinhardt, S., R. L. C. Vink, and F. Schmid. 2013. Monolayer curva-ture stabilizes nanoscale raft domains in mixed lipid bilayers. *Proc. Natl. Acad. Sci. USA.* 110:4476–4481.

21. Parthasarathy, R., C. H. Yu, and J. T. Groves. 2006. Curvature-modu-lated phase separation in lipid bilayer membranes. *Langmuir.* 22:5095–5099.

22. Parthasarathy, R., and J. T. Groves. 2007. Curvature and spatial organi-zation in biological membranes. *Soft Matter.* 3:24–33.

23. Veatch, S. L., and S. L. Keller. 2003. Separation of liquid phases in gi-ant vesicles of ternary mixtures of phospholipids and cholesterol. *Biophys. J.* 85:3074–3083.

24. Helfrich, W. 1973. Elastic properties of lipid bilayers: theory and possible experiments. *Z. Naturforsch. C.* 28:693–703.

25. Hansen, P., L. Miao, and J. Ipsen. 1998. Fluid lipid bilayers: intermo-nolayer coupling and its thermodynamic manifestations. *Phys. Rev. E Stat. Phys. Plasmas Fluids Relat. Interdisc. Topics.* 58:2311–2324.

26. Sunil Kumar, P. B., G. Gompper, and R. Lipowsky. 1999. Modulated phases in multicomponent fluid membranes. *Phys. Rev. E Stat. Phys. Plasmas Fluids Relat. Interdisc. Topics.* 60:4610–4618.

27. Leibler, S., and D. Andelman. 1987. Ordered and curved meso-struc-tures in membranes and amphiphilic films. *J. Phys.* 48:2013–2018.

28. Andelman, D., T. Kawakatsu, and K. Kawasaki. 1992. Equilibrium shape of two-component unilamellar membranes and vesicles. *Euro-phys. Lett.* 19:57–62.

29. Gozdz, W. T., and G. Gompper. 2001. Shape transformations of two--component membranes under weak tension. *Europhys. Lett.* 55: 587–593.

30. Harden, J. L., F. C. MacKintosh, and P. D. Olmsted. 2005. Budding and domain shape transformations in mixed lipid films and bilayer mem-branes. *Phys. Rev. E Stat. Nonlin. Soft Matter Phys.* 72:011903.

31. MacKintosh, F. C. 1994. Mixed fluid bilayers: effects of confinement. *Phys. Rev. E Stat. Phys. Plasmas Fluids Relat. Interdisc. Topics.* 50:2891–2897.

32. Weikl, T. R., D. Andelman, …, R. Lipowsky. 2002. Adhesion of mem-branes with competing specific and generic interactions. *Eur. Phys. J E Soft Matter.* 8:59–66.

33. Lin, L. C. L., and F. L. H. Brown. 2004. Brownian dynamics in Fourier space: membrane simulations over long length and time scales. *Phys. Rev. Lett.* 93:256001.

34. Tröster, A. 2007. Coarse grained free energies with gradient corrections from Monte Carlo simulations in Fourier space. *Phys. Rev. B.* 76:012402.

35. Virnau, P., and M. Müller. 2004. Calculation of free energy through successive umbrella sampling. *J. Chem. Phys.* 120:10925–10930.

36. Ferrenberg, A. M., and R. H. Swendsen. 1989. Optimized Monte Carlo data analysis. *Phys. Rev. Lett.* 63:1195–1198.

37. Toner, J., and D. Nelson. 1981. Smectic, cholesteric, and Rayleigh-Be-nard order in two dimensions. *Phys. Rev. B.* 23:316–334.

38. Newman, M. E. J., and G. T. Barkema. 1999. Monte Carlo Methods in Statistical Physics. Clarendon Press, Oxford, UK.

39. Vollmayr, K., J. D. Reger, …, K. Binder. 1993. Finite size effects at thermally-driven first order phase transitions: a phenomenological the-ory of the order parameter distribution. *Z. Phys. B.* 91:113–125.

40. Lee, J., and J. M. Kosterlitz. 1991. Finite-size scaling and Monte Carlo simulations of first-order phase transitions. *Phys. Rev. B Condens. Mat-ter.* 43:3265–3277.

41. Binder, K. 1982. Monte Carlo calculation of the surface tension for two- and three-dimensional lattice-gas models. *Phys. Rev. A.* 25:1699–1709.

42. Orkoulas, G., A. Z. Panagiotopoulos, and M. E. Fisher. 2000. Criti-cality and crossover in accessible regimes. *Phys. Rev. E Stat. Phys. Plasmas Fluids Relat. Interdisc. Topics.* 61 (5B):5930–5939.

43. Binder, K., and D. P. Landau. 1984. Finite-size scaling at first-order phase transitions. *Phys. Rev. B.* 30:1477–1485.

44. Binder, K. 1997. Applications of Monte Carlo methods to statistical physics. *Rep. Prog. Phys.* 60:487–559.

45. Müller, M., and K. Binder. 2001. Interface localization-delocalization transition in a symmetric polymer blend: a finite-size scaling Monte Carlo study. *Phys. Rev. E Stat. Nonlin. Soft Matter Phys.* 63:021602.

46. Anisimov, M. A., A. F. Kostko, …, I. K. Yudin. 2005. Competition of mesoscales and crossover to θ-point tricriticality in near-critical poly-mer solutions. *J. Chem. Phys.* 123:164901.

47. Wilding, N. B., and P. Nielaba. 1996. Tricritical universality in a two-dimensional spin fluid. *Phys. Rev. E Stat. Phys. Plasmas Fluids Relat. Interdisc. Topics.* 53:926–934.

48. Toulmay, A., and W. A. Prinz. 2013. Direct imaging reveals stable, micrometer-scale lipid domains that segregate proteins in live cells. *J. Cell Biol.* 202:35–44.

49. Lingwood, D., and K. Simons. 2010. Lipid rafts as a membrane-orga-nizing principle. *Science.* 327:46–50.

50. Gompper, G., and M. Schick. 1990. Lattice model of microemulsions: the effect of fluctuations in one and two dimensions. *Phys. Rev. A.* 42:2137–2149.

51. Shlomovitz, R., L. Maibaum, and M. Schick. 2014. Macroscopic phase separation, modulated phases, and microemulsions: a unified picture of rafts. *Biophys. J.* 106:1979–1985.

52. Sadeghi, S., and R. L. C. Vink. 2012. Main transition in the Pink membrane model: finite-size scaling and the influence of surface roughness. *Phys. Rev. E Stat. Nonlin. Soft Matter Phys.* 85:061912.

53. Corvera, E., M. Laradji, and M. J. Zuckermann. 1993. Application of finite-size scaling to the Pink model for lipid bilayers. *Phys. Rev. E Stat. Phys. Plasmas Fluids Relat. Interdiscip. Topics.* 47:696–703.